

Processive movement of single kinesins on crowded microtubules visualized using quantum dots

Arne Seitz and Thomas Surrey*

European Molecular Biology Laboratory (EMBL), Cell Biology and Biophysics Unit, Heidelberg, Germany

Kinesin-1 is a processive molecular motor transporting cargo along microtubules. Inside cells, several motors and microtubule-associated proteins compete for binding to microtubules. Therefore, the question arises how processive movement of kinesin-1 is affected by crowding on the microtubule. Here we use total internal reflection fluorescence microscopy to image *in vitro* the runs of single quantum dot-labelled kinesins on crowded microtubules under steady-state conditions and to measure the degree of crowding on a microtubule at steady-state. We find that the runs of kinesins are little affected by high kinesin densities on a microtubule. However, the presence of high densities of a mutant kinesin that is not able to step efficiently reduces the average speed of wild-type kinesin, while hardly changing its processivity. This indicates that kinesin waits in a strongly bound state on the microtubule when encountering an obstacle until the obstacle unbinds and frees the binding site for kinesin's next step. A simple kinetic model can explain quantitatively the behaviour of kinesin under both crowding conditions.

The EMBO Journal (2006) 25, 267–277. doi:10.1038/sj.emboj.7600937; Published online 12 January 2006

Subject Categories: membranes & transport

Keywords: crowding; molecular motors; quantum dots; single-molecule imaging

Introduction

Motor proteins are mechanochemical enzymes whose movement along filaments is powered by ATP hydrolysis. Kinesin-1 (or conventional kinesin) is a microtubule-dependent motor protein that was the founding member for a large protein superfamily (Dagenbach and Endow, 2004). Kinesin-1 moves towards the microtubule plus end in a processive manner. This means that it makes several consecutive steps without detaching from the microtubule. Inside cells, Kinesin-1 transports various cargos such as vesicles, organelles, protein complexes, virus particles, and mRNAs (Hirokawa, 1998; Hirokawa *et al.*, 1998; Schliwa and Woehlke, 2003). It is a heterotetramer consisting of two heavy chains and two light chains (Vale, 2003). The minimal functional unit for processive movement is a homodimer of

about the first 400 amino acids of the heavy chain (Hackney, 1994a). This sequence contains the N-terminal motor domain (also called a head) and a subsequent coiled coil leading to dimerization.

Kinesin-1 is the best-studied motor of the kinesin superfamily, and its basic kinetic properties are quite well understood. Its biochemical cycle consists essentially of the binding of one head to the microtubule, subsequent binding and hydrolysis of ATP at this head, release of phosphate from this bound head and release of ADP from the second head (Hackney, 1996; Gilbert *et al.*, 1998; Moyer *et al.*, 1998) with concomitant strong binding of the second head to the microtubule, and only then dissociation of the first head from the microtubule (Hackney, 1994a; Rosenfeld *et al.*, 2003; Cross, 2004; Klumpp *et al.*, 2004). This starts the cycle again on the newly bound head. The precise mechanochemical coupling of the enzymatic cycles of the two heads is the prerequisite for kinesin's property to walk processively in a hand-over-hand manner (Asbury *et al.*, 2003; Schliwa, 2003; Schief *et al.*, 2004; Yildiz *et al.*, 2004). Kinesin makes on average about 100 steps before it dissociates from its track. During each biochemical cycle the centre of mass of the dimeric molecule is moved by a characteristic step size of 8 nm corresponding to the size of an α/β -tubulin heterodimer.

In the crowded environment inside living cells, various kinesins, dynein and several nonmotile microtubule-associated proteins (MAPs) compete for binding to microtubules. Under such conditions, kinesins moving along microtubules are expected to frequently encounter obstacles on their path. Surprisingly little is known about how interactions with other proteins influence the motility of kinesins. It could be shown previously by observing single fluorescent kinesin molecules that neuronal MAPs did not influence the velocity or processivity of Kinesin-1 (Seitz *et al.*, 2002). This at that time unexpected finding can now be better understood because cryo-electron microscopy experiments showed that these MAPs and kinesin bind to different sites on the microtubule (Santarella *et al.*, 2004). Fundamentally different interfering effects on kinesin motility can be expected if proteins block the kinesin-binding site on the microtubule. Therefore, the question arises how such obstacles, for example other kinesins on the same protofilament of a microtubule, affect kinesin's mechanochemical properties like its speed or processivity (Crevel *et al.*, 2004). This question has, however, not been addressed yet under steady-state conditions. Especially, single-molecule observations of kinesin that can provide a wealth of kinetic information have not yet been performed under controlled conditions of crowding. It is therefore unclear if in such a case kinesin would unbind or wait when encountering an obstacle. Answers to this question can have important implications for cargo transport along crowded microtubules by kinesins inside living cells.

Here we used total internal reflection fluorescence (TIRF) microscopy to measure *in vitro* how single kinesins move

*Correspondence: EMBL, Cell Biology and Biophysics Unit, Meyerhofstrasse 1, 69117 Heidelberg, Germany.
Tel.: +49 6221 387 8360; Fax: +49 6221 387 8512;
E-mail: surrey@embl.de

Received: 11 July 2005; accepted: 6 December 2005; published online: 12 January 2006

along single microtubules in the presence of high concentrations of competing motors. To be able to observe precisely how long individual runs of single kinesins are and how much time the kinesins need for individual runs, we labelled the kinesins with quantum dots (Chan *et al.*, 2002). These semiconductor nanocrystals offer the advantage of highly increased photostability as compared to conventional fluorophores like Cy3 or eGFP that are commonly used for single-molecule imaging. We were interested in the consequences of two crowding conditions on kinetic parameters like the binding rate, the speed, the processivity and the dwell time of kinesin. We first measured if wild-type kinesins at high concentrations on the microtubule affected each other's motility, addressing the question of whether traffic jams were generated on crowded microtubules by statistical kinesin velocity variations. We then measured how high concentrations of a kinesin mutant with a motility defect affected the motility of single wild-type kinesins, addressing the question of whether Kinesin-1 waits or detaches from the microtubule when it encounters a roadblock.

Results

Quantum dots as labels to record single-kinesin motility

To be able to follow accurately single kinesin dimers during their entire runs along a crowded microtubule from the binding to the unbinding event, we decided to use quantum dots as extremely photostable fluorescent probes. This eliminated problems of photobleaching that might obscure part of the run. We labelled biotinylated conventional kinesins with streptavidin-coated quantum dots (see Materials and methods) and observed their motility by TIRF microscopy (Figure 1A). Kymographs (time-space plots) showed that individual runs had roughly constant velocity (Figure 1B). In agreement with single-molecule studies of kinesins labelled with fluorophores (Friedman and Vale, 1999; Inoue *et al.*, 2001) (Supplementary Figure 1), the velocities that were measured for many individual runs showed a Gaussian distribution with a mean velocity of around $0.6 \mu\text{m/s}$, and the run lengths of the individual runs showed an exponential distribution with an overall average run length of around $1 \mu\text{m}$ (Figure 1C).

To ensure that the quantum dots that we observed were predominantly moved by single kinesins, we performed a control experiment in which we varied the ratio of kinesins per quantum dot. Similar to previous experiments with micrometer beads (Block *et al.*, 1990; Klopfenstein *et al.*, 2002), we observed that increasing kinesin to quantum dot ratios did not affect significantly the velocity, but clearly increased the travel distance of the kinesin-coated quantum dots (Figure 1D). At low ratios around and below 1 kinesin monomer, that is, 0.5 kinesin dimers per quantum dot, typical single-molecule behaviour was observed. The value for the average run length under these conditions is in good agreement with results of measurements of single conventional kinesin motility using standard fluorophores (Vale *et al.*, 1996; Romberg *et al.*, 1998; Thorn *et al.*, 2000; Inoue *et al.*, 2001) (see also Supplementary Figure 1). We therefore used a kinesin to quantum dot ratio of around 1 for all experiments of this study, if not stated otherwise.

Our results demonstrate that quantum dots can be used to monitor the movement of single kinesins along microtubules.

Owing to their photostability, long run lengths and long dwell times of kinesins on microtubules can be measured accurately.

Binding of kinesin-GFP to microtubules under steady-state conditions

The aim of this study was to measure how motor crowding on a microtubule affects the motility of Kinesin-1 under steady-state conditions. It was therefore important to first determine quantitatively the densities of walking motors on a microtubule. We measured steady-state densities by TIRF microscopy using a kinesin-GFP fusion protein (Figure 2A and B) under experimental conditions that we later used for motility experiments. As expected, the dissociation constant $K_{D,MT}$ of kinesin-GFP was significantly higher in the presence of ATP than in the presence of AMP-PNP. The $K_{D,MT}$ of about 200 nM for kinesin-GFP in the presence of ATP was in a similar range as measured before for GFP-free kinesin by microtubule cosedimentation (Hackney, 1994b). Interestingly, we found that the maximum density on a microtubule was reduced by about a factor of two for kinesins walking in the presence of ATP as compared to kinesins being statically bound to the microtubule in the presence of the nonhydrolysable ATP analogue AMP-PNP (Figure 2B). This reflects nicely the difference between a dynamic and a static situation.

Cryo-electron microscopy studies have shown that in the presence of AMP-PNP, binding ratios of one kinesin dimer per one tubulin heterodimer (Arnal and Wade, 1998; Hirose *et al.*, 1999) or per two tubulin heterodimers can be observed (Hoenger *et al.*, 1998; Skiniotis *et al.*, 2003). Intermediate binding ratios were also reported under certain conditions (Hoenger *et al.*, 2000; Skiniotis *et al.*, 2003), indicating that probably the details of the binding kinetics are important for the exact binding stoichiometry (Vilfan *et al.*, 2001). Therefore, we estimate that in our experiment with AMP-PNP at the maximum kinesin density probably some of the kinesin dimers are attached via only one head to the microtubule, while some others are attached with both heads corresponding to a maximum binding ratio being at most 1:1 and at least 1:2. This means that the maximum binding ratio in the presence of ATP was at most 1:2 and at least 1:4 (Figure 2B).

Motility of single kinesins on crowded microtubules

As individual conventional kinesins move with rather varying velocities, resulting in a broad velocity distribution (Figure 1C) (Romberg *et al.*, 1998; Yajima *et al.*, 2002; Kaseda *et al.*, 2003), the question arises if kinesins interfere with each other when moving at high densities on a microtubule. We asked whether the fraction of faster moving kinesins is slowed down by the fraction of the slower moving kinesins under conditions of crowding on the microtubule. Or, if instead faster kinesins dissociate earlier from a microtubule, once they reach a more slowly moving kinesin. Such effects would cause a decrease of the average velocity or of the average run length.

Adding high concentrations of kinesin-GFP to quantum dot-labelled kinesins allowed us to both follow the motility of the quantum dot-labelled kinesins along microtubules and to measure the occupancy of the microtubules with kinesin-GFP. We found that increasing the concentration of kinesin-GFP to $0.9 \mu\text{M}$ strongly decreased the binding frequency of

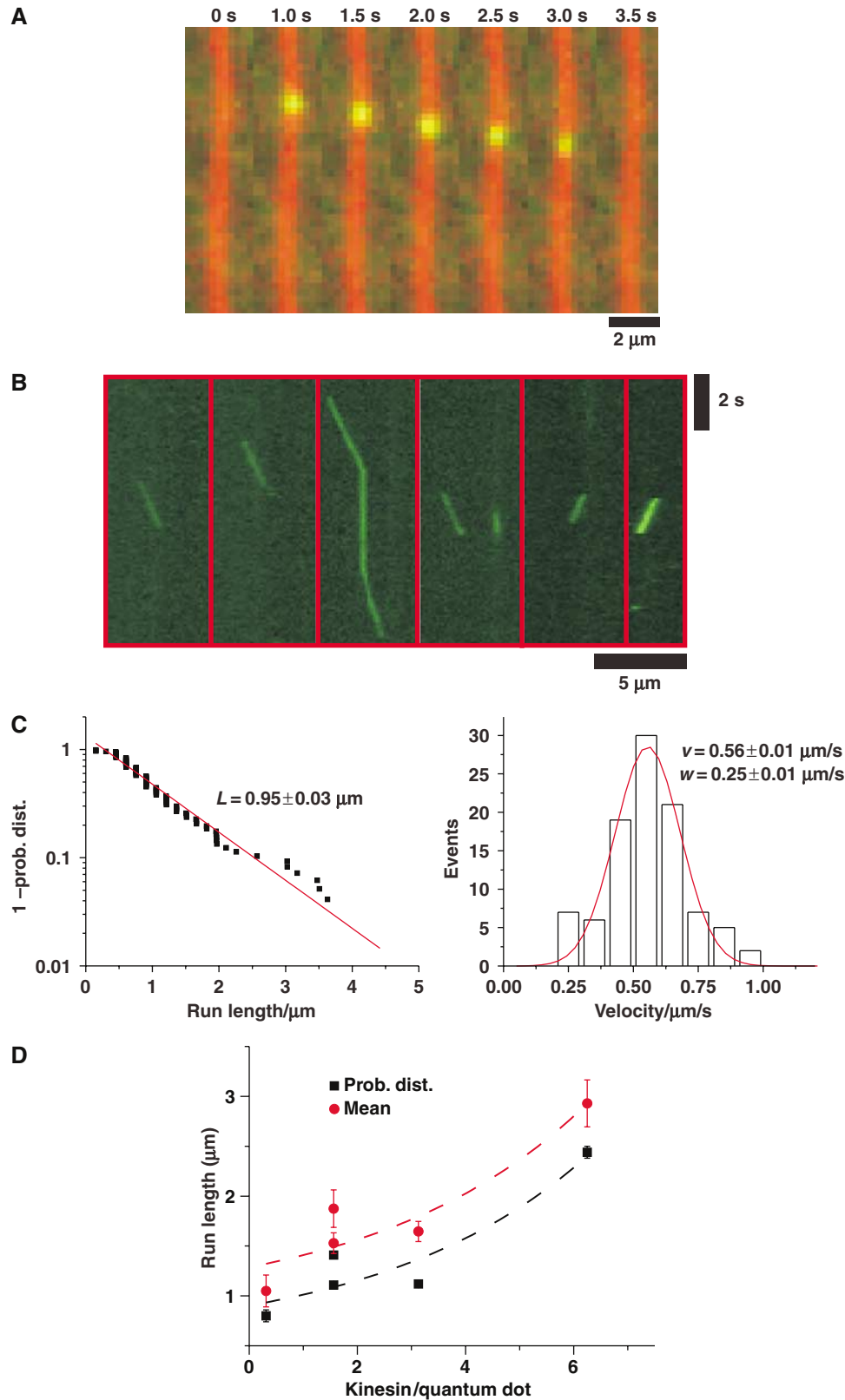


Figure 1 Motility of kinesins coupled to quantum dots. (A) TIRF microscopy of quantum dot-labelled kinesins (green) moving along Texas Red-labelled microtubules (red). Concentrations were 5 nM biotinylated kinesin, 5 nM streptavidin-coated quantum dots, and 2 mM MgATP. Images of one microtubule at different time points are shown. The bar is 2 μm . (B) Kymographs of quantum dot-labelled kinesins moving along six different microtubules. Diagonal lines with constant slope represent runs with constant speed, while vertical lines represent immobile or pausing quantum dots. (C) Probability distribution of the individual run lengths of quantum dot-labelled kinesins with a linear regression yielding the average run length (left), and velocity histogram with a Gaussian fit yielding the average velocity (right) (see Materials and methods). (D) Average run lengths of kinesin-quantum dot conjugates at different kinesin-quantum dot mixing stoichiometries. Average run lengths were obtained either from a fit to the probability distribution of the individual run lengths (black squares, with black bars for the error of the fit) or as the mean of the run lengths (red circles with red bars for the standard deviation). The lines represent exponential fits to the data.

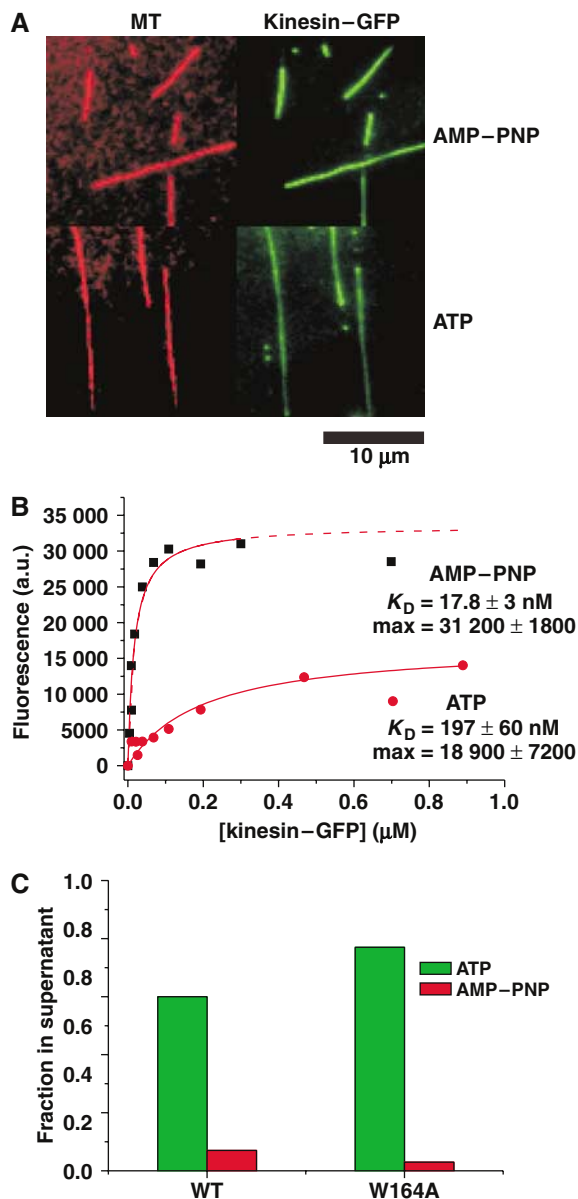


Figure 2 Binding of kinesin to microtubules. (A) TIRF microscopy of 150 nM kinesin-GFP (green) binding to surface-immobilized Texas Red-labelled microtubules (red) in the presence of 2 mM MgAMP-PNP (top) and in the presence of 2 mM MgATP (bottom). The bar is 10 μ m. (B) Fluorescence intensities of kinesin-GFP bound to microtubules in the presence of 2 mM MgATP (red circles) and 2 mM MgAMP-PNP (black squares) at varying concentrations of kinesin-GFP, as measured by TIRF microscopy. The concentration of microtubules on the surface was estimated to be less than 1 nM. Red curves are hyperbolic fits assuming thermodynamic equilibrium binding (see Materials and methods). (C) Percentage of unbound kinesin after cosedimentation of 1 μ M wild-type kinesin (left) or 1 μ M E164A mutant (right) with 2 μ M microtubules in the presence of 2 mM MgATP (green) or 2 mM MgAMP-PNP (red). Both wild-type and mutant kinesin were released to a large extent from the microtubules in the presence of MgATP, while they bind strongly in the presence of MgAMP-PNP.

quantum dot-labelled kinesins, reflecting the decreased number of available binding sites on the microtubule (Figure 3A). This decrease in the binding frequency was in good agreement with the $K_{D,MT}$ that was measured by TIRF microscopy (compare Figure 3A left with Figure 2B). We did, however,

not observe a strong change in the average velocity (Figure 3B), in the average run length (Figure 3C), or in the average dwell time (Figure 3D) of quantum dot-labelled kinesins with increasing kinesin-GFP concentrations. Similarly, the distributions of these kinetic parameters did not change significantly. This was the case for quantum dots with single kinesins (Figure 3, left column) and for quantum dots with multiple kinesins (Figure 3, right column). Judged from the measured K_D 's and the concentrations used in these experiments, we were able to measure the velocity, travel distance, and dwell time up to an occupancy of about 60–70% of the maximum occupancy on the microtubule. In the presence of ATP, this corresponds to an occupancy of at most one kinesin dimer being bound per three tubulin dimers. These results indicate that kinesin's motility is quite insensitive to crowding up to this occupancy under these experimental conditions.

Motility of single kinesins in the presence of obstacles

To better understand this apparent insensitivity of Kinesin-1 to crowding on the microtubule, we tested what conventional kinesin does under steady-state conditions when it encounters an obstacle that reversibly blocks the next binding site along its track. Therefore, we recorded the movement of quantum dot-labelled kinesins in the presence of increasing concentrations of unlabelled mutant motors (mutant E164A of *Drosophila* conventional kinesin). This mutant cannot hydrolyse ATP at the second head (Klumpp *et al*, 2004) and therefore shows severely inhibited motility (Klumpp *et al*, 2003). The steady-state ATP turnover rate of 5 s^{-1} and the ability to make at most one step suggest a dwell time of 200 ms on the microtubule. A cosedimentation experiment confirmed that the mutant does not irreversibly bind to microtubules in the presence of ATP (Figure 2C). Compared with wild-type kinesin that makes 50–100 steps per second (i.e. 1 step per 10–20 ms), this mutant makes 1 step per 200 ms and acts therefore as an obstacle with a 10–20-fold increased residence time at a binding site. We measured how the presence of these obstacles on a microtubule interfered with the motility of quantum dot-labelled wild-type kinesins.

Increasing the concentration of the E164A mutant to 1.75 μ M caused the binding frequency of quantum dot-labelled wild-type kinesins (Figure 4A) to decrease by about 90%. This decrease of the binding frequency again reflects the reduced number of available binding sites on the decorated microtubule. The decrease in the binding frequency agrees with a $K_{D,MT}$ of 440 nM, which is slightly higher than the $K_{D,MT}$ of kinesin-GFP (see also Figure 2C and Supplementary Figure 2). Given this $K_{D,MT}$ for the mutant, we expect an occupancy close to saturation of the microtubule with the mutant kinesin at the highest mutant concentration used in our experiment. Increasing the concentration of the added mutant to 1.75 μ M caused the average velocity of quantum dot-labelled wild-type kinesins to decrease by roughly a factor of 10 (Figure 4B), while the run length was hardly affected (Figure 4C). In agreement with these two last results, the dwell time increased approximately by a factor of 10 (Figure 4D).

Taken together, these results indicate that kinesin waits when encountering an obstacle along its track until the obstacle unbinds and frees the track again. Then kinesin

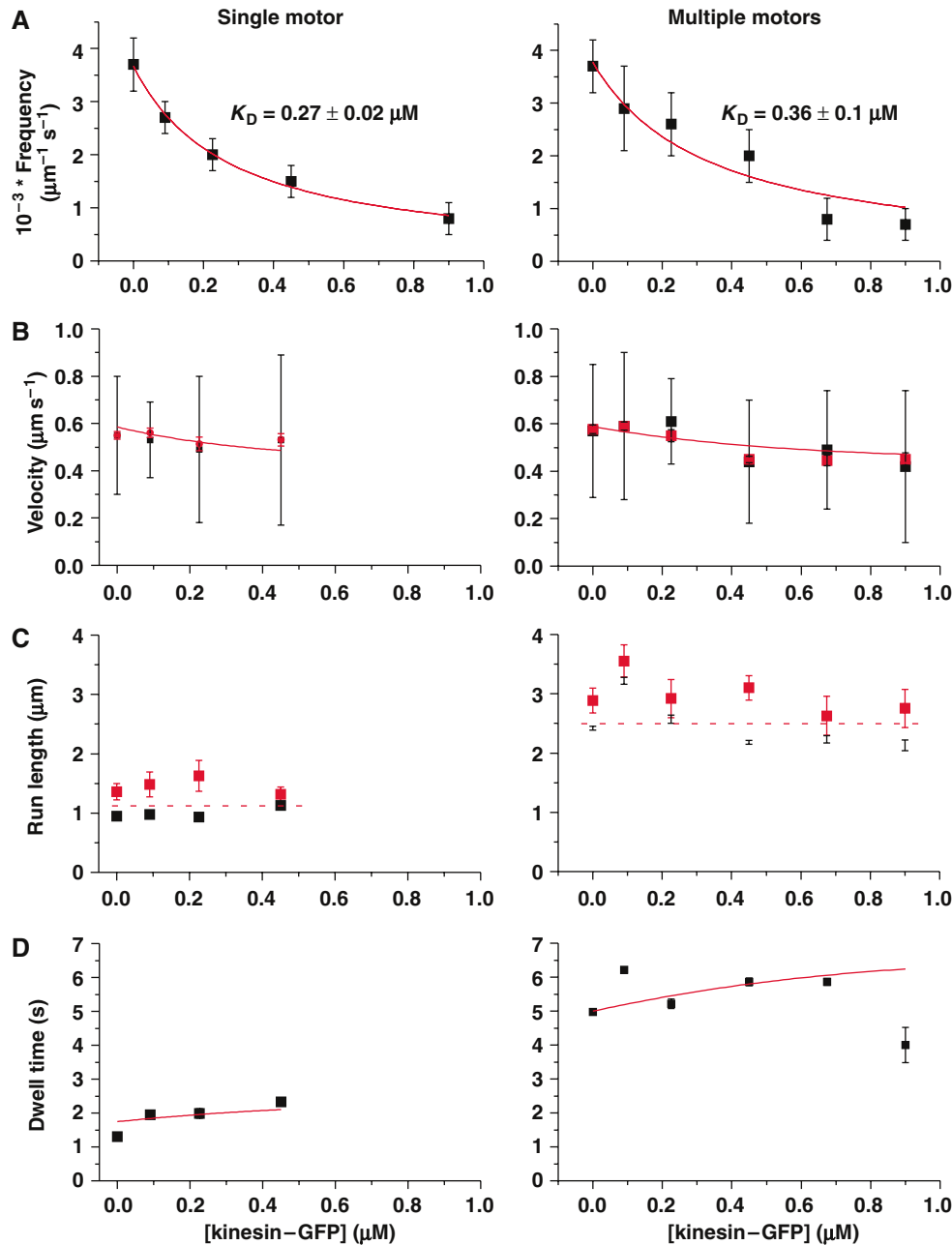


Figure 3 Effect of kinesin-GFP on the motility of quantum dot-labelled single kinesins and of kinesin clusters. Motility parameters of the runs of 1 nM streptavidin-coated quantum dots associated with 1 nM biotinylated kinesin (left column: single motors) and 5 nM biotinylated kinesin (right column: multiple motors) in the presence of 0–0.9 μM kinesin-GFP and 2 mM MgATP. (A) Frequency of binding of quantum dot-labelled kinesins to microtubules (black squares) and the calculated error (black bars). (B) Average velocity of quantum dot-labelled kinesins calculated from a Gaussian fit to the velocity distribution (black squares) with standard deviation (red bars), and mean velocities (red circles) with standard deviation (red bars). (C) Average run length as obtained from a fit to the probability distribution of the individual run lengths (black squares), and mean travel distance (red circles) with standard deviation (red bars). (D) Average dwell time as obtained from a fit to the probability distribution of the individual dwell times (black squares) and the error of the fit parameter (black bars, not visible in most cases). The red lines are fits to the kinetic parameters at different kinesin-GFP concentrations based on the kinetic model illustrated in Figure 5 and as described in Materials and methods.

continues its walk until it encounters the next obstacle or finally unbinds and ends its run. It should be noted that the individual episodes of running and waiting are not resolved under our experimental conditions. Interestingly, the run length of kinesin is largely unaffected despite an increasing fraction of the time that kinesin spends waiting. This indicates that kinesin waits in a strongly bound state (see Discussion).

We note that our steady-state single-molecule observations differ from results obtained in light-scattering experiments (Crevel *et al.*, 2004). In these experiments, wild-type kinesins were arrested on microtubules in a strongly bound rigour state in the absence of nucleotide and in the presence of roadblocks, probably well above steady-state densities. Wild-type kinesins were then released from the microtubule by addition of ATP, causing the system to relax into a dynamic

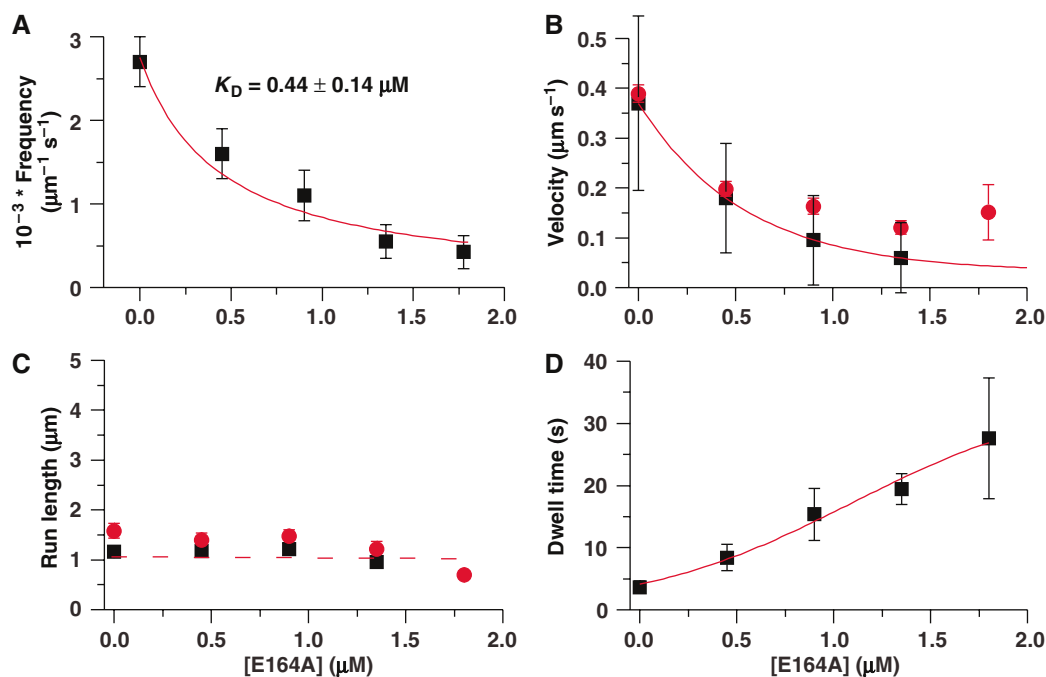


Figure 4 Effect of the mutant E164A on the motility of single quantum dot-labelled wild-type kinesins. Motility parameters of the runs of 1 nM quantum dots associated with 1 nM biotinylated wild-type kinesins in the presence of 0–1.6 μM mutant E164A and 2 mM MgATP. **(A)** Binding frequency of single quantum dot-labelled wild-type kinesins to microtubules (black squares) and the calculated error (black bars). **(B)** Average velocity of single quantum dot-labelled wild-type kinesins, as calculated from a Gaussian fit of the velocity distribution (black squares) plotted together with the standard deviation of the fitted distribution (black bars), and the mean velocities (red circles) plotted together with their standard deviation (red bars). **(C)** Average run length as obtained from a fit to the probability distribution of the individual run lengths (black squares), and the mean run length (red circles) with the standard deviation (red bars). **(D)** Average dwell time as obtained from a fit to the probability distribution of the individual dwell times (black squares) and the error of the fit parameter (black bars). The red lines are fits to the kinetic parameters at different mutant E164A concentrations based on the kinetic model illustrated in Figure 5 and as described in Materials and methods. Note the different scale of the abscissa as compared to Figure 3.

steady-state situation. Starting from these overcrowded conditions, kinesins appeared to perform only very short runs of few steps, while the system relaxed to steady-state. The difference to our results most likely reflects the different characteristics of this relaxation process from a trapped state into steady-state (Vugmeyster *et al.*, 1998). Further experiments will be required to fully explain this difference.

Discussion

We studied how the movement of conventional kinesin was affected by crowding on the microtubule. To visualize single kinesins, we attached them to quantum dots and followed their runs by single-molecule imaging using TIRF microscopy. Velocity distributions and run length distributions typical for single kinesins were measured with quantum dot-labelled motors (Figure 1). Using these semiconductor nanocrystals instead of conventional fluorophores allowed us to accurately measure the long dwell times of the kinesins on the microtubule, because the observation time was not limited by photobleaching. Blinking of the quantum dots that has been reported before was strongly repressed by the use of a reducing agent in our experiments (Hohng and Ha, 2004).

Owing to their brightness, the use of quantum dots for labelling kinesins allowed us to follow single molecules (labelled with quantum dots) in the presence of high concentrations of other fluorescently labelled proteins that were added as crowding agents. The presence of a fluorescence

label on the crowding agent had the advantage of allowing us to measure the degree of crowdedness on the microtubule by TIRF microscopy under exactly the same steady-state conditions under which the runs of quantum dot-labelled kinesins were observed. An important first result was the observation that the maximum density of kinesins under steady-state conditions, that is, when kinesins move along the microtubule, was considerably lower as compared to a static situation in the presence of AMP-PNP (Figure 2B), where densities of either one kinesin dimer per tubulin dimer or per two tubulin dimers have been reported in cryo-electron microscopy experiments (Arnal and Wade, 1998; Hirose *et al.*, 1999; Hoenger *et al.*, 2000; Skiniotis *et al.*, 2003). Therefore, our binding curves indicate that the maximum steady-state density of kinesin-GFPs walking on a microtubule in the presence of ATP is at most one kinesin dimer per two tubulin dimers and at least one kinesin dimer per four tubulin dimers. Our results reflect nicely the difference in occupancy between a dynamic steady-state and a static arrested state.

Motivated by the situation in the living cell, the main goal of this study was to examine at steady-state conditions, that is, in the presence of high ATP concentrations, how crowding on the microtubule affects the runs of individual kinesins. We tested in two series of experiments the effect of high densities of wild-type kinesins and of mutant kinesins with a motility defect on the movements of single quantum dot-labelled wild-type kinesins. The mutant kinesin E164A (Klump *et al.*, 2003, 2004) can be seen as a roadblock that reversibly

binds to a binding site on the microtubule without being able to step efficiently. It unbinds from this binding site and then probably also from the microtubule with a rate of 5 s^{-1} , while wild-type kinesin moves on a free microtubule from one binding site to the next binding site at a rate that is one order of magnitude faster, and unbinds from the microtubule after having made on average about 100 steps. Independent of the type of crowding agent (wild-type kinesin or mutant kinesin), we found that the binding rate of quantum dot-labelled kinesins was strongly decreased by both crowding agents, simply reflecting the reduction in the number of available binding sites on the microtubule. This result is similar to earlier studies with neuronal MAPs (Seitz *et al*, 2002). Furthermore, also independent of the crowding agents that we tested, the processivity of quantum dot-labelled kinesins was hardly affected. Different effects were, however, observed on the average velocity and dwell time of quantum dot-labelled kinesins. While wild-type kinesins had no strong effect on the velocity and dwell time of quantum dot-labelled kinesins, the reversible roadblock mutant significantly slowed down wild-type kinesins and concurrently increased their dwell time on the microtubule.

To understand these results, one needs to consider kinesin's biochemical cycle. It consists of a set of transitions between several different microtubule-bound states. During the cycle, the kinesin heads have different affinities for the microtubule, depending mainly on their nucleotide state. The rates of the transitions between the states vary considerably, allowing the distinction between rate-limiting and non-rate-limiting steps. Most kinetic models of kinesin can be approximated for the purpose of this discussion by a simplified kinetic scheme consisting of only two states. Kinesin is strongly bound to the microtubule in one of these two states (state S in Figure 5A), representing either the nucleotide-free or the ATP-bound state. Unbinding of kinesin from the microtubule in either of these states is very slow, with unbinding rates of 0.001 s^{-1} (Hancock and Howard, 1999). We therefore neglect unbinding from the strongly bound state here. When kinesin is, however, tethered via one ADP- and/or Pi-bound head to the microtubule, it can dissociate from its track (and end the cycle) at a rate of $k_{\text{off}} = 1 \text{ s}^{-1}$ (Hancock and Howard, 1999), representing therefore a weakly bound state (state W in Figure 5A). At high ATP concentrations, the transition from the strongly bound state S to the weakly bound state W is fast, at a rate $k_1 = 4000 \text{ s}^{-1}$ (at high concentrations of 1 mM ATP, which we assume throughout this discussion). The weakly bound state W is the most populated state, because its transition to the next state, during which kinesin's second head binds the next binding site and releases hydrolysis products, is the rate-limiting step of the cycle with $k_2 = 50\text{--}100 \text{ s}^{-1}$. In which order exactly hydrolysis products are released is still a matter of debate. Most models favour a mechanism in which phosphate is released first (Rosenfeld *et al*, 2003; Cross, 2004; Klumpp *et al*, 2004), while others claim that ADP is released first (Schief *et al*, 2004). The releases of the two hydrolysis products are included in our simplified kinetic scheme in the transition associated with the slow rate k_2 . The overall velocity of kinesin is in this model determined by the two rates k_1 and k_2 . In the absence of obstacles (and at high ATP concentrations), k_2 is rate-limiting. The average number of consecutive steps that kinesin makes, that is, its processivity,

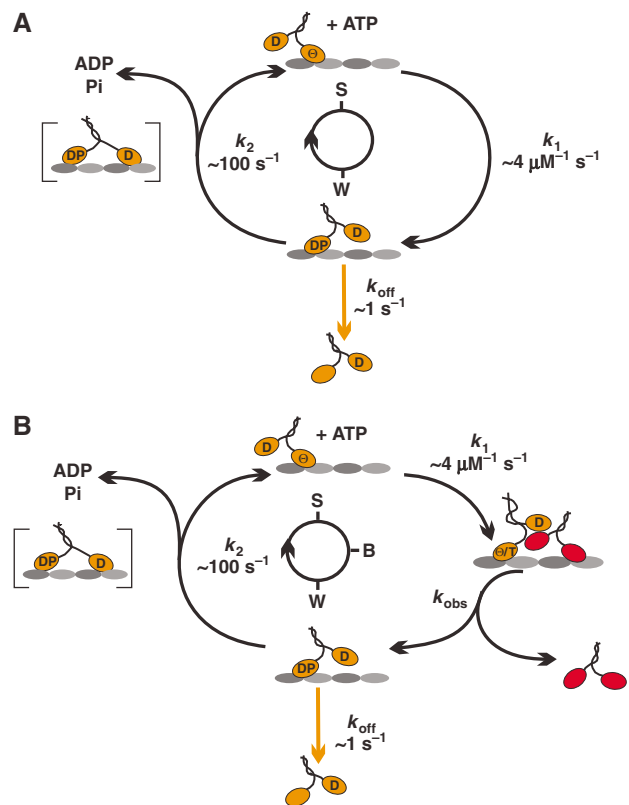


Figure 5 Simplified model for kinesin's biochemical cycle. Biochemical cycle with a strongly bound state S and a weakly bound state W of wild-type kinesin (orange) in the absence (A) and the presence (B) of an obstacle (red). The obstacle blocks kinesin in a strongly bound state B. The slow reverse reactions are neglected. The intermediate in brackets indicates that a real cycle consists of several more than two intermediates, which are omitted here for simplicity.

is determined in this model by the ratio of the competing unbinding rate k_{off} and the forward binding rate k_2 .

The observation that the reversible roadblock E164A slowed down the average velocity of wild-type kinesin without affecting its processivity strongly suggests that kinesin waits in a strongly bound state (state B in Figure 5B) when encountering an obstacle. It probably waits in a nucleotide-free or ATP-bound state, both known to be strongly bound states. Once the obstacle detaches from the microtubule, kinesin can now perform a fast conformational change that is otherwise blocked in the presence of the obstacle, and it continues its walk until it encounters the next obstacle.

Based on this interpretation, the experimental data of the crowding experiment with the E164A mutant can be explained quantitatively. We assume that the binding frequency decreases proportionally with the occupancy δ of the microtubule with obstacles, and that the occupancy δ in turn is determined by the $K_{\text{D,MT}}$ and the concentration of the obstacles. Then, we can fit the decrease of the binding frequency of quantum dot-labelled motors with an equation in which the $K_{\text{D,MT}}$ of the obstacle is a free fitting parameter (Figure 4A; see Materials and methods). We furthermore assume for kinesin's average velocity v the equation $v = (1 - \delta)v_{\text{free}} + \delta v_{\text{blocked}}$. This expresses the velocity as an average between the velocity v_{free} for a biochemical cycle in the case of a free next binding site and the velocity v_{blocked} for

a biochemical cycle in the case of a blocked next binding site. v_{free} and v_{blocked} are expressed as functions of the rates k_1 , k_2 and the unbinding rate k_{obs} of the obstacles (see Materials and methods). We assume here that the weights of the velocities of a 'free' cycle and a 'blocked' cycle in the average are given by the occupancy δ . The average dwell time T can now be expressed as $T = L/v$, with L being the run length. The experimental data of the average velocities (Figure 4B) and of the average dwell times (Figure 4D) of quantum dot-labelled motors at different obstacle concentrations can now be fitted using these expressions, having $K_{\text{D,MT}} = 0.44 \mu\text{M}$ (taken from the fit of the decrease of the binding frequency) and $k_1 = 4000 \text{ s}^{-1}$ (Schief *et al*, 2004) as fixed parameters and k_2 , k_{obs} and L as free parameters. The fit results in $k_2 = 42 \text{ s}^{-1}$, $k_{\text{obs}} = 7.6 \text{ s}^{-1}$ and $L = 1.6 \mu\text{m}$ (Supplementary Table 1), which are in fair agreement with the expected values of 75 s^{-1} (from our measured speed of $0.6 \mu\text{m/s}$), 5 s^{-1} (Klumpp *et al*, 2003), and $1 \mu\text{m}$ (our measured run length), respectively.

How can one now understand that kinesin is rather insensitive to crowding of the microtubule with wild-type kinesins (Figure 3)? If the forward step of a wild-type kinesin is blocked by the presence of another wild-type kinesin at the next binding site, this 'wild-type obstacle' will in most of the cases free this binding site with its forward stepping rate $k_2 = 50\text{--}100 \text{ s}^{-1}$. This much faster rate of freeing the blocked site as compared to the E164A mutant already indicates that less drastic effects on the velocity and dwell time of quantum dot-labelled motors can be expected in this case. As 'wild-type obstacles' free the blocked binding site by stepping to a next binding site (and not by dissociating from the microtubule like the E164A mutant), the rate at which they free the next binding site is expected to be subject to crowding effects especially at high occupancies, and therefore not to be independent of the occupancy (Lipowsky *et al*, 2001). However, velocities, run lengths, and dwell times at such very high occupancies could not be measured in our steady-state experiment with wild-type kinesins. The main reason is that in the dynamic situation of a steady-state, kinesins walking in the presence of saturating ATP concentrations can only partially decorate the microtubule (Figure 2B). Furthermore, average velocities, run lengths, and dwell times could only be measured reliably, if the binding frequency was not too low. As a first approximation, we therefore used the same kinetic model for the experiments in which the wild-type kinesins acted as obstacles to fit the data.

We determined an apparent $K_{\text{D,MT}}$ of 270 nM from the fit of the decrease of the binding frequencies of single kinesins with increasing 'wild-type obstacle' concentrations (Figure 3A, left column). This $K_{\text{D,MT}}$ was in good agreement with the $K_{\text{D,MT}}$ determined in the binding measurement by means of TIRF microscopy (Figure 2B). As the microtubule is at most only half decorated with kinesins when this binding curve 'saturates' in the presence of high ATP concentrations, the maximum occupancy is set to 0.5 for the quantitative analysis of crowding experiments with wild-type kinesins. The experimental data of the average velocities (Figure 3B) and of the average dwell times (Figure 3D) of quantum dot-labelled motors at different 'wild-type obstacle' concentrations can now be fitted satisfactorily using these expressions having $K_{\text{D,MT}}$ (taken from the fits of the binding frequencies) and $k_1 = 4000 \text{ s}^{-1}$ (Schief *et al*, 2004) as fixed parameters and having $k_2 = k_{\text{obs}}$ and L as free parameters. The fit results in

$k_2 = k_{\text{obs}} = 74 \text{ s}^{-1}$, being in agreement with our measured speeds of quantum dot-labelled kinesins and of kinesin-GFP (Supplementary Figure 1). The fit also results in values for the run lengths that agree with $L = 1.0 \mu\text{m}$ and $2.9 \mu\text{m}$, with the experimentally determined values for the single quantum dot-labelled motors (Figure 3C, left column) and for multiple motor quantum dots (Figure 3C, right column), respectively (all results from the fits are summarized in Supplementary Table 1).

Our results are in agreement with kinetic models of kinesin's biochemical cycle (e.g., Hackney, 2002; Yajima *et al*, 2002; Schief *et al*, 2004) that can be approximated: (1) by a two-state model with a strongly bound and a weakly bound state and where (2) kinesin's processivity is determined by the ratio of the competing unbinding rate k_{off} and the forward stepping rate k_2 , which are the two rates for the two transitions kinesin can undergo from the weakly bound state.

Unchanged processivity under crowding conditions is in this model a consequence of kinesin's property to wait in a strongly bound state when encountering an obstacle (instead of waiting in the weakly bound state). Obstacles that free the blocked site considerably more slowly than an undisturbed kinesin usually occupies a binding site, lead to a reduced average velocity and an increased dwell time of the walking motors. The moderate effect, however, that crowding the microtubule with similarly fast processive motors has on the average velocity and dwell time is a consequence of both the similarity of the speeds and the fact that moving kinesins prevent full decoration of the microtubule.

This ability to wait without detaching from the microtubule enables kinesin to function even under crowded conditions. With respect to its function as a transporter of cargo such as a vesicle along a microtubule in the presence of various molecules competing for binding sites, these properties could be advantageous for efficient transport in the crowded environment of a living cell. The property of a motor to wait and not to unbind from the microtubule when encountering an obstacle might be the reason why various types of vesicles that are transported by motors along microtubules have been observed to pause in living cells, perhaps because static obstacles block the track for considerable time (Scales *et al*, 1997; Kaether *et al*, 2000; Lalli and Schiavo, 2002).

Materials and methods

Protein biochemistry

The proteins were expressed and purified as described elsewhere: Biotinylated kinesin (Surrey *et al*, 1998) is a fusion of the first 401 amino acids of wild-type *Drosophila* conventional kinesin with biotin carboxyl carrier protein. Kinesin-GFP (Seitz *et al*, 2002) is a fusion of the first 555 amino acids of wild-type rat conventional kinesin and GFP. The mutant E164A (Klumpp *et al*, 2003) consists of the first 401 amino acids of *Drosophila* conventional kinesin, with amino acid E164 being replaced by A. For cosedimentation controls, a corresponding wild-type construct without this mutation was used. Biotinylated kinesin and kinesin-GFP were both microtubule affinity purified (Seitz *et al*, 2002). The kinesin concentrations were determined by Bradford using BSA as standard, and are expressed as monomer concentrations.

The purification of tubulin from pig brain, the Texas Red labelling of tubulin, and the polymerization of microtubules were performed as described (Hyman *et al*, 1991; Castoldi and Popov,

2003). The tubulin concentrations were determined by UV absorption and are expressed as dimer concentrations.

For the cosedimentation experiments, 1 μM kinesin (wild-type or E164A) was mixed with 2 μM of microtubules in 20 mM Pipes, pH 6.9, containing 50 mM NaCl, 1 mM MgCl_2 , 1 mM EGTA, 10 mM β -mercaptoethanol, and 40 μM paclitaxel. After adding either MgATP or MgAMP-PNP to a final concentration of 2 mM, the sample was centrifuged for 15 min at room temperature with 174 000 g. A control sample containing no microtubules was treated identically, demonstrating that the kinesins did not aggregate (data not shown). Supernatants were analysed by SDS-PAGE, Coomassie staining, and densitometry of the bands.

Preparation of quantum dot-labelled kinesins moving on microtubules

A flow cell was constructed using ethanol-cleaned coverslips and a double sticky tape (Tesa). The surface of the flow cell was approximately $5 \times 5 \text{ mm}^2$ and its volume was approximately 5 μl . In all, 1 cell volume of 50–100 $\mu\text{g/ml}$ polyclonal tubulin antibody (ab1289, abcam) was flowed into the cell. After 5 min incubation the cell was washed with 2 cell volumes of T12 (12 mM K-Pipes, 1 mM EGTA, 2 mM MgCl_2 , 20 μM paclitaxel, pH 6.8) followed by 1 cell volume of Texas Red-labelled microtubules (0.5 μM tubulin in T12). After 1 min incubation, nonimmobilized microtubules were washed out with 2 cell volumes of TC12 (0.5 mg/ml casein (C-6905, SIGMA) in T12). Then, 4 cell volumes of motor mix were flowed through the cell. The motor mix consisted of 0.5–2 nM biotinylated kinesins labelled with streptavidin-coated quantum dots (Qdot 585 nm, Quantum Dot Corp.), 1–5 mM MgATP, and 10 mM β -mercaptoethanol in TC12 buffer. We used a mixing ratio of one kinesin (monomer!) per quantum dot, that is, half a kinesin dimer per quantum dot for single-motor recordings. Under these conditions, it follows from Poisson statistics (Block *et al.*, 1990) that more than 70% of quantum dots have no motor bound, that about 30% of quantum dots have one motor bound, and that less than 10% of quantum dots have two (or more) motors bound. We furthermore estimate a reach of several nm for our short biotinylated kinesin construct. Thus, simultaneous binding of two kinesins on the same quantum dot of about 15–20 nm diameter to a microtubule can be expected for less than 30% of all quantum dots covered with two kinesins. This means that 10% or less of all quantum dot–kinesin conjugates (not counting quantum dots without kinesins) might be bound via two kinesins to the microtubule. Given the short average run lengths and monoexponential distributions of the individual run lengths that we observe experimentally, we think that this might even be an overestimate and conclude that the large majority of runs are single-molecule runs.

For one experiment with quantum dots coated with multiple motors, we used a mixing ratio of 5 (Figure 3, right column). Interfering motors were included in the motility mix at varying concentrations ranging from 0 to 1 μM for kinesin–GFP and from 0 to 1.75 μM for the mutant E164A.

Controls: (1) We varied the mixing ratio between 0.25 and 6 kinesins per quantum dot, keeping the quantum dot concentration at 1 nM (in the absence of interfering motors) (Figure 1D). (2) Kinesin–GFP and the E164A mutant were mixed at 1 and 1.5 μM , respectively, with quantum dots (2 nM) in the absence of biotinylated kinesin. These quantum dots did not show movement or binding to microtubules (data not shown), demonstrating that neither kinesin–GFP nor E164A attached nonspecifically to the quantum dots. (3) We measured the concentration of kinesin–GFP in the flow cell by flowing out the final solution containing 0.5 and 1 μM kinesin–GFP at the end of our standard protocol. The concentration of kinesin recovered from the cell was 90–95% of the original concentration of the solution applied to the flow cell as determined by SDS-PAGE (data not shown). This control demonstrates that there was no significant depletion of added interfering kinesins in the flow cell due to nonspecific adsorption to the glass surface.

Binding curves measured by TIRF microscopy

Microtubules were bound to the surface of a flow cell as described above. Then, 4 cell volumes of 5–1000 nM kinesin–GFP in TC12 with 1 mM Mg-nucleotide and 10 mM β -mercaptoethanol were flowed through the cell. The fluorescence intensity of kinesin–GFP was measured by TIRF microscopy (see below). To determine the GFP intensity of kinesin–GFP associated with the microtubule, a

line scan (with a width of 1 pixel) was performed along the microtubule with ImageJ and an identical background line scan was performed next to the microtubule. The intensity of the background scan was then subtracted to correct for the background signal. The average fluorescence intensity $I(c)$ of microtubule-bound kinesin–GFP was determined from 20 to 40 microtubules for each of several kinesin–GFP concentrations c . As kinesin–GFPs are in large excess over microtubules ($< 1 \text{ nM}$ polymerized tubulin), the concentration of unbound kinesin can be approximated by the concentration of total kinesin. The $K_{D,MT}$ value was obtained from a fit of a hyperbola to a plot of $I(c)$ versus c (Figure 2B), using $I(c) = I_{\text{max}} \cdot c / (K_D + c)$, where I_{max} is the fluorescence intensity of kinesin–GFP at saturation.

TIRF microscopy

Kinesins and microtubules were observed at room temperature on an inverted microscope (IX71, Olympus) equipped with a TIRF condenser (IX2-REVA TIRF, Olympus), an objective (PLAPO60XO/TIRFM-SP/1.45, Olympus) suitable for TIRF illumination through the objective, and an on-chip integration camera (Cascade, VisiTron). Evanescent excitation of quantum dots was achieved using either the 405 nm line of a diode-pumped solid-state laser (Compass 405, Coherent) or the 488 nm line of an argon ion laser (IMA 101, Melles Griot). The 488 nm line was also used for excitation of kinesin–GFP. Texas Red-labelled microtubules were excited using the 532 nm line of a diode-pumped solid-state laser (Compass 215M, Coherent).

After the position of the microtubules was recorded, moving quantum dots were recorded in the same field of view every 50–200 ms for a total period of 60–90 s. Metamorph was used for image acquisition and the control of shutters and of an acousto-optical tuneable filter.

Data analysis

For each run of a quantum dot-labelled kinesin to be analysed, a time–space plot (kymograph) was created along the trace of the microtubule, using a self-written Plug-In for ImageJ. In the kymographs moving kinesins were identified as straight lines (Figure 1B), with attachment and detachment positions and times being clearly detectable. Occasional transitions from motility to pausing were regarded as the end of runs, while occasional transitions from pausing to moving were considered as the start of runs. The pausing frequency did not depend on the degree of crowding. Using this information obtained from the kymographs we calculated the velocity, the travel distance, and the dwell time of the individual kinesins. To calculate the average velocity, the average travel distance, and the average dwell time of an ensemble of kinesins, at least 100 runs per condition were analysed. The average velocity was obtained by fitting a Gaussian distribution to a histogram with the frequencies of the velocities of the individual runs. This histogram was created by binning the velocities of the individual runs into equally spaced containers and plotting the number of events against the median of the container. To calculate the average travel distance, a single exponential was fitted to the cumulative probability distribution of the individual travel distances (Thorn *et al.*, 2000). The average travel distance equals the decay constant of the exponential fitting function. Average dwell times were derived by the same procedure. Arithmetic mean values of the velocity and of the travel distance were also calculated for control purposes. For calculating the binding frequency, the total number of runs along 30–100 microtubules was divided by the length of the individual microtubules and by the time of observation.

To analyse the dependence of these average kinetic parameters on the occupancy of the microtubule with crowding motors, we used a simple kinetic model (Figure 5). We performed nonlinear least-square fits for the dependence of the binding frequencies f on the concentration c of the crowding agents (Figures 3A and 4A), using the equation $f(c) = (1 - \delta(c)) \cdot f_{\text{max}}$, with f_{max} being the binding frequency for empty microtubules and occupancy δ being $\delta(c) = \delta_{\text{max}} \cdot c / K_D + c$. The maximum occupancy was set to $\delta_{\text{max}} = 1$ for the E164A mutant and to $\delta_{\text{max}} = 0.5$ for kinesin–GFP as obstacles (see Figure 2B). Using the values for the dissociation constants K_D that resulted from these fits, we then performed a global nonlinear least-square fit of the dependence of the velocity and, simultaneously, of the dwell time on the concentration of crowding motors. For the velocity (Figures 3B and 4B), we used the equation $v(c) = (1 - \delta(c)) \cdot v_{\text{free}} + \delta(c) \cdot v_{\text{blocked}}$. This velocity is an average of:

(a) the velocity of motors stepping onto a free next binding site $v_{\text{free}} = s \cdot (k_1 \cdot k_2) / (k_1 + k_2)$ (Figure 5A) and of (b) the velocity of motors having to wait for an obstacle to free the next binding site

$$v_{\text{blocked}} = s \cdot \frac{k_1 \cdot k_2}{(k_1 \cdot k_2) / k_{\text{obs}} + k_1 + k_2}$$

(Figure 5B) (Hill, 1989), with s being the step size of 8 nm. This average is assumed to be weighted by the occupancy δ . For the dwell time T (Figures 3D and 4D), we used the equation $T(c) = L / v(c)$, with L being the run length. All nonlinear least-square fits were performed with Origin.

References

- Arnal I, Wade RH (1998) Nucleotide-dependent conformations of the kinesin dimer interacting with microtubules. *Structure* **6**: 33–38
- Asbury CL, Fehr AN, Block SM (2003) Kinesin moves by an asymmetric hand-over-hand mechanism. *Science* **302**: 2130–2134
- Block SM, Goldstein LS, Schnapp BJ (1990) Bead movement by single kinesin molecules studied with optical tweezers. *Nature* **348**: 348–352
- Castoldi M, Popov AV (2003) Purification of brain tubulin through two cycles of polymerization–depolymerization in a high-molarity buffer. *Protein Expr Purif* **32**: 83–88
- Chan WC, Maxwell DJ, Gao X, Bailey RE, Han M, Nie S (2002) Luminescent quantum dots for multiplexed biological detection and imaging. *Curr Opin Biotechnol* **13**: 40–46
- Crevel IM, Nyitrai M, Alonso MC, Weiss S, Geeves MA, Cross RA (2004) What kinesin does at roadblocks: the coordination mechanism for molecular walking. *EMBO J* **23**: 23–32
- Cross RA (2004) The kinetic mechanism of kinesin. *Trends Biochem Sci* **29**: 301–309
- Dagenbach EM, Endow SA (2004) A new kinesin tree. *J Cell Sci* **117**: 3–7
- Friedman DS, Vale RD (1999) Single-molecule analysis of kinesin motility reveals regulation by the cargo-binding tail domain. *Nat Cell Biol* **1**: 293–297
- Gilbert SP, Moyer ML, Johnson KA (1998) Alternating site mechanism of the kinesin ATPase. *Biochemistry* **37**: 792–799
- Hackney DD (1994a) Evidence for alternating head catalysis by kinesin during microtubule-stimulated ATP hydrolysis. *Proc Natl Acad Sci USA* **91**: 6865–6869
- Hackney DD (1994b) The rate-limiting step in microtubule-stimulated ATP hydrolysis by dimeric kinesin head domains occurs while bound to the microtubule. *J Biol Chem* **269**: 16508–16511
- Hackney DD (1996) The kinetic cycles of myosin, kinesin, and dynein. *Annu Rev Physiol* **58**: 731–750
- Hackney DD (2002) Pathway of ADP-stimulated ADP release and dissociation of tethered kinesin from microtubules. Implications for the extent of processivity. *Biochemistry* **41**: 4437–4446
- Hancock WO, Howard J (1999) Kinesin's processivity results from mechanical and chemical coordination between the ATP hydrolysis cycles of the two motor domains. *Proc Natl Acad Sci USA* **96**: 13147–13152
- Hill TL (1989) *Free Energy Transduction and Biochemical Cycle Kinetics*. New York: Springer-Verlag
- Hirokawa N (1998) Kinesin and dynein superfamily proteins and the mechanism of organelle transport. *Science* **279**: 519–526
- Hirokawa N, Noda Y, Okada Y (1998) Kinesin and dynein superfamily proteins in organelle transport and cell division. *Curr Opin Cell Biol* **10**: 60–73
- Hirose K, Lowe J, Alonso M, Cross RA, Amos LA (1999) Congruent docking of dimeric kinesin and ncd into three-dimensional electron cryomicroscopy maps of microtubule–motor ADP complexes. *Mol Biol Cell* **10**: 2063–2074
- Hoenger A, Doerhoefer M, Woehlke G, Tittmann P, Gross H, Song YH, Mandelkow E (2000) Surface topography of microtubule walls decorated with monomeric and dimeric kinesin constructs. *Biol Chem* **381**: 1001–1011
- Hoenger A, Sack S, Thormahlen M, Marx A, Muller J, Gross H, Mandelkow E (1998) Image reconstructions of microtubules

Supplementary data

Supplementary data are available at *The EMBO Journal* Online.

Acknowledgements

We thank Susan P Gilbert for the kind gift of E164A, Eckhard Mandelkow for the vector of kinesin–GFP, Mathias Utz for technical assistance, Stefan Klumpp, Robert A Cross and François Nédélec for stimulating discussions, and the VolkswagenStiftung for financial support.

- decorated with monomeric and dimeric kinesins: comparison with X-ray structure and implications for motility. *J Cell Biol* **141**: 419–430
- Hohng S, Ha T (2004) Near-complete suppression of quantum dot blinking in ambient conditions. *J Am Chem Soc* **126**: 1324–1325
- Hyman A, Drechsel D, Kellogg D, Salser S, Sawin K, Steffen P, Wordeman L, Mitchison T (1991) Preparation of modified tubulins. *Methods Enzymol* **196**: 478–485
- Inoue Y, Iwane AH, Miyai T, Muto E, Yanagida T (2001) Motility of single one-headed kinesin molecules along microtubules. *Biophys J* **81**: 2838–2850
- Kaether C, Skehel P, Dotti CG (2000) Axonal membrane proteins are transported in distinct carriers: a two-color video microscopy study in cultured hippocampal neurons. *Mol Biol Cell* **11**: 1213–1224
- Kaseda K, Higuchi H, Hirose K (2003) Alternate fast and slow stepping of a heterodimeric kinesin molecule. *Nat Cell Biol* **5**: 1079–1082
- Klopfenstein DR, Tomishige M, Stuurman N, Vale RD (2002) Role of phosphatidylinositol(4,5)bisphosphate organization in membrane transport by the Unc104 kinesin motor. *Cell* **109**: 347–358
- Klumpp LM, Brendza KM, Rosenberg JM, Hoenger A, Gilbert SP (2003) Motor domain mutation traps kinesin as a microtubule rigour complex. *Biochemistry* **42**: 2595–2606
- Klumpp LM, Hoenger A, Gilbert SP (2004) Kinesin's second step. *Proc Natl Acad Sci USA* **101**: 3444–3449
- Lalli G, Schiavo G (2002) Analysis of retrograde transport in motor neurons reveals common endocytic carriers for tetanus toxin and neurotrophin receptor p75NTR. *J Cell Biol* **156**: 233–239
- Lipowsky R, Klumpp S, Nieuwenhuizen TM (2001) Random walks of cytoskeletal motors in open and closed compartments. *Phys Rev Lett* **87**: 108101
- Moyer ML, Gilbert SP, Johnson KA (1998) Pathway of ATP hydrolysis by monomeric and dimeric kinesin. *Biochemistry* **37**: 800–813
- Romberg L, Pierce DW, Vale RD (1998) Role of the kinesin neck region in processive microtubule-based motility. *J Cell Biol* **140**: 1407–1416
- Rosenfeld SS, Fordyce PM, Jefferson GM, King PH, Block SM (2003) Stepping and stretching. How kinesin uses internal strain to walk processively. *J Biol Chem* **278**: 18550–18556
- Santarella RA, Skiniotis G, Goldie KN, Tittmann P, Gross H, Mandelkow EM, Mandelkow E, Hoenger A (2004) Surface-decoration of microtubules by human tau. *J Mol Biol* **339**: 539–553
- Scales SJ, Pepperkok R, Kreis TE (1997) Visualization of ER-to-Golgi transport in living cells reveals a sequential mode of action for COPII and COPI. *Cell* **90**: 1137–1148
- Schief WR, Clark RH, Crevenna AH, Howard J (2004) Inhibition of kinesin motility by ADP and phosphate supports a hand-over-hand mechanism. *Proc Natl Acad Sci USA* **101**: 1183–1188
- Schliwa M (2003) Kinesin: walking or limping? *Nat Cell Biol* **5**: 1043–1044
- Schliwa M, Woehlke G (2003) Molecular motors. *Nature* **422**: 759–765
- Seitz A, Kojima H, Oiwa K, Mandelkow EM, Song YH, Mandelkow E (2002) Single-molecule investigation of the interference between kinesin, tau and MAP2c. *EMBO J* **21**: 4896–4905
- Skiniotis G, Surrey T, Altmann S, Gross H, Song YH, Mandelkow E, Hoenger A (2003) Nucleotide-induced conformations in the neck region of dimeric kinesin. *EMBO J* **22**: 1518–1528

- Surrey T, Elowitz MB, Wolf PE, Yang F, Nedelec F, Shokat K, Leibler S (1998) Chromophore-assisted light inactivation and self-organization of microtubules and motors. *Proc Natl Acad Sci USA* **95**: 4293–4298
- Thorn KS, Ubersax JA, Vale RD (2000) Engineering the processive run length of the kinesin motor. *J Cell Biol* **151**: 1093–1100
- Vale RD (2003) The molecular motor toolbox for intracellular transport. *Cell* **112**: 467–480
- Vale RD, Funatsu T, Pierce DW, Romberg L, Harada Y, Yanagida T (1996) Direct observation of single kinesin molecules moving along microtubules. *Nature* **380**: 451–453
- Vilfan A, Frey E, Schwabl F, Thormahlen M, Song YH, Mandelkow E (2001) Dynamics and cooperativity of microtubule decoration by the motor protein kinesin. *J Mol Biol* **312**: 1011–1026
- Vugmeyster Y, Berliner E, Gelles J (1998) Release of isolated single kinesin molecules from microtubules. *Biochemistry* **37**: 747–757
- Yajima J, Alonso MC, Cross RA, Toyoshima YY (2002) Direct long-term observation of kinesin processivity at low load. *Curr Biol* **12**: 301–306
- Yildiz A, Tomishige M, Vale RD, Selvin PR (2004) Kinesin walks hand-over-hand. *Science* **303**: 676–678